



Isotropic Reconstruction of 3D EM Images with Unsupervised Degradation Learning

Shiyu Deng¹, Xueyang Fu^{1(✉)}, Zhiwei Xiong¹, Chang Chen¹, Dong Liu¹,
Xuejin Chen¹, Qing Ling², and Feng Wu¹

¹ University of Science and Technology of China, Hefei, China
xyfu@ustc.edu.cn

² Sun Yat-sen University, Guangzhou, China

Abstract. The isotropic reconstruction of 3D electron microscopy (EM) images with low axial resolution is of great importance for biological analysis. Existing deep learning-based methods rely on handcrafted down-scaled training data, which does not model the real degradation accurately and thus leads to unsatisfying performance in practice. To address this problem, we propose a universal and unsupervised framework to simultaneously learn the real axial degradation and the isotropic reconstruction of 3D EM images. First, we train a degradation network using unpaired low-resolution (LR) and high-resolution (HR) slices, both of which are from real data, in an adversarial manner. Then, the degradation network is further used to generate realistic LR data from HR labels to form paired training data. In this way, the generated degraded data is consistent with the real axial degradation process, which guarantees the generalization ability of subsequent reconstruction networks to the real data. Our framework has the flexibility to work with different existing reconstruction methods. Experiments on both simulated and real anisotropic EM images validate the superiority of our framework.

Keywords: Isotropic reconstruction · Unsupervised learning · EM image

1 Introduction

Three dimensional electron microscopy (EM) imaging reveals biological information at a scale of nanometer, which makes it possible for ultrastructural analysis. It is desirable to have a consistent resolution across all dimensions, both for visualization and for biological analysis tasks. In practice, however, most EM techniques such as serial section Transmission EM (ssTEM) and block-face scanning EM fail to obtain the desired high axial resolution [17]. Generally, the axial (z) resolution is of one magnitude lower compared with the lateral (x , y) resolution. Although Focused Ion Beam Scanning EM (FIB-SEM) can achieve 8–10 nm resolution in all the x , y , z directions, it takes an unaffordable long time

to image a large volume sample [8]. Therefore, it is of great demand to replace the time-consuming imaging with an effective reconstruction method to obtain high-quality isotropic 3D EM images.

To increase the resolution along the axial direction of 3D EM images, traditional interpolation methods are widely used due to their straightforward operations. Although these methods are simple and efficient, they usually result in images with severe volume artifacts, which hinders the subsequent processing and analysis [27]. Recently, deep learning-based methods have achieved significant improvements on both natural images restoration [2,3,12,15,23] and biomedical images analysis [5,18]. There also emerge a few works aiming to recover isotropic EM images with the deep learning framework. As a representative, Heinrich et al. [10] compared two 3D convolutional neural networks (CNNs), which are trained in a supervised manner on artificially down-scaled isotropic FIB-SEM images for 3D EM super-resolution. Their results indicate that inferring high-resolution (HR) structures from low-resolution (LR) EM images is possible. However, the isotropic ground truth images of the same category are not always available, and these supervised 3D CNNs may not generalize well to EM images that are drastically different from the training data in content. This domain shift issue poses a common challenge for existing supervised CNNs-based methods.

Along the other line, Weigert et al. [20,21] proposed a self-supervised deep learning method to restore isotropic fluorescence volumes from anisotropic optical acquisitions, where the restoration process is modeled as a combination of a super-resolution problem on sub-sampled data and a deconvolution problem to counteract the microscopy induced optical point spread function (PSF). Most importantly, they introduced the concept of self super-resolution, i.e., training and testing on the same anisotropic volumetric data. Similar ideas have also been explored for isotropic reconstruction of magnetic resonance images in [4,27,28]. Although self-supervised methods do not require isotropic ground truth training data, which may cause potential domain shift issues, these methods require prior knowledge of the PSF. In practice, however, this degradation is unknown and could be drastically different from the handcrafted designed ones, which again restricts the generalization ability of the above methods in real scenarios.

Theoretically, the real degradation along the axial direction can be exactly learned by CNNs trained on realistic axial HR-LR pairs. Nevertheless, this kind of axial HR-LR pairs are difficult to acquire, which makes supervised learning not feasible. In this paper, inspired by unpaired learning for natural image processing [1,22,29,30], we propose a framework with unsupervised degradation learning for isotropic reconstruction of 3D EM images. Different from those methods on 2D natural images, we design our framework for the 3D volume. Specifically, our framework contains a degradation model and a reconstruction model. To train the degradation model, we adopt unpaired HR lateral and LR axial images from a single, anisotropic 3D EM volume as training data. We assume that the biological structure in the 3D volume conforms to an isotropic distribution (i.e. the cell body is spherical). In this way, using the unpaired training strategy, the trained

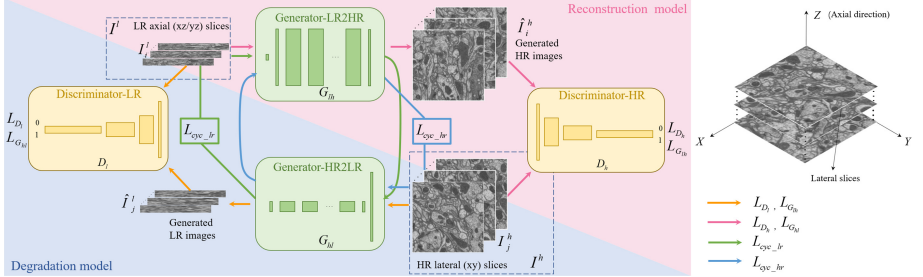


Fig. 1. Overview of our framework. G_{hl} aims to generate LR image \hat{I}_j^l from the real HR image I_j^h ; G_{lh} aims to restore HR image \hat{I}_i^h from the real LR image I_i^l . The generated LR image \hat{I}_j^l and real LR image I_i^l are used to train the discriminator D_l ; the generated HR image \hat{I}_i^h and real HR image I_j^h are used to train the discriminator D_h .

model can generate down-scaled slices that are close to those from the real axial degradation. The generated LR images paired with original HR images are further fed into the reconstruction model to learn the reconstruction function. This makes our framework easy to train and can be directly applied to anisotropic data. Thus, neither the domain shift issue in previous supervised methods nor the mismatch of the degradation in previous self-supervised methods will exist, which greatly improves the generalization ability of our framework in practice. Experiments demonstrate notably improved numerical and perceptual results of our framework over existing solutions, and a state-of-the-art neuron segmentation method is evaluated on the reconstructed isotropic volume, which further validate the superiority of our framework on the subsequent analysis. Moreover, the proposed framework is agnostic to the reconstruction network backbones, and a wide range of super-resolution networks can be plugged in. Furthermore, the proposed framework can be readily applied to isotropic reconstruction of other 3D biomedical images.

This paper has the following contributions: 1) We propose a universal and unsupervised framework, in which both the real axial degradation and the reconstruction can be jointly learned, for isotropic reconstruction of 3D EM images. 2) We prove that the generalization ability of our framework can be guaranteed since neither external training data nor degradation assumptions are needed. 3) Within our framework, users can arbitrarily choose the restoration method, which increase the flexibility of our framework. Experiments on both simulated and real anisotropic EM data validate the superiority of our framework.

2 Methodology

Overall Architecture. As shown in Fig. 1, our framework includes a degradation model and a reconstruction model, both of which consist of a generator and a discriminator. In the degradation model, we use unpaired HR lateral (xy) and LR axial (xz/yz) slices from an anisotropic 3D EM volume to train the

generator, which aims to simulate the real degradation process and generate LR images. In the reconstruction model, the generator aims to restore HR images from LR axial (xz/yz) slices. The two discriminators try to distinguish between real or generated images, and the two generators try to fool the corresponding discriminator. Therefore, the discriminators and generators are jointly trained in an adversarial manner. In this way, the trained generator is able to capture the true data distribution [7], which enables it to produce realistic LR images as new training data.

Specifically, given an anisotropic 3D EM volume I , we denote the LR axial slices as I^l , and the HR lateral slices as I^h . The degradation model and the reconstruction model learn the mappings between I^l and I^h . As shown in Fig. 1, using the j^{th} HR image I_j^h as input, the generator G_{hl} down-scales it into an LR image \hat{I}_j^l . Similarly, using the i^{th} LR image I_i^l as input, the generator G_{lh} super-resolves it into an HR image \hat{I}_i^h . The generated LR image \hat{I}_j^l and real LR image I_i^l are used to train the discriminator D_l , while \hat{I}_i^h and I_j^h are used to train the discriminator D_h . In addition, as shown by the green and blue circles, we also add cycle-consistent losses to force the backward mapping to bring the generated image back to the original for stable training. At the testing phase, only G_{lh} is used for super-resolving I_i^l . Since our framework is able to receive unpaired images from different sources as training data, neither the domain shift issue in previous supervised methods nor the mismatch of the degradation in previous self-supervised methods will exist.

Network Implementation. The degradation model consists of the generator G_{hl} and the discriminator D_l . The generator G_{hl} uses ResNet [9] as the backbone structure. Specifically, we first adopt an average pooling layer to down-scale the input resolution 10 times along the vertical (y) direction, followed by 9 residual blocks to generate the LR image. Similar to [15], we remove the batch normalization. We set the kernel size as 3×3 , and each convolution layer includes 64 filters. For the discriminator D_l , we stack 4 stride convolution layers, which followed by Leaky ReLU activation, along the horizontal (x) direction. The kernel size is set to 3×7 to adapt to the resolution of input images.

The reconstruction model consists of G_{lh} and D_h . The generator G_{lh} increases the resolution of an input image 10 times along the vertical direction. To guarantee the restoration quality, universal super-resolution networks can be used as G_{lh} . To be simple and effective, by default, the generator G_{lh} contains a linear interpolation in the front of the network, and 9 residual blocks are then used to learn the non-linear mapping for HR detail restoration. We refer to this Default ReConstruction network as *DRCNet*. For the discriminator D_h , we adopt the architecture of PatchGAN [14,30] to relieve the computation burden.

Loss Function. We adopt adversarial losses to guide the training of both HR to LR mapping and LR to HR mapping. Specifically, we use a least-squares loss [16]. For the HR to LR mapping: $I^h \rightarrow I^l$, we formulate the objective as

$$\mathcal{L}_{G_{hl}} = \mathbb{E}_{I_j^h \sim P(I^h)} \|D_l(G_{hl}(I_j^h)) - 1\|_2. \quad (1)$$

For the discriminator D_l , we have

$$\mathcal{L}_{D_l} = \mathbb{E}_{I_i^l \sim P(I^l)} \|D_l(I_i^l) - 1\|_2 + \mathbb{E}_{I_j^h \sim P(I^h)} \|D_l(G_{hl}(I_j^h))\|_2. \quad (2)$$

Similarly, for the LR to HR mapping: $I^l \rightarrow I^h$, we have

$$\mathcal{L}_{G_{lh}} = \mathbb{E}_{I_i^l \sim P(I^l)} \|D_h(G_{lh}(I_i^l)) - 1\|_2. \quad (3)$$

For the discriminator D_h , we have

$$\mathcal{L}_{D_h} = \mathbb{E}_{I_j^h \sim P(I^h)} \|D_h(I_j^h) - 1\|_2 + \mathbb{E}_{I_i^l \sim P(I^l)} \|D_h(G_{lh}(I_i^l))\|_2. \quad (4)$$

According to [30], using only adversarial losses cannot guarantee that the learned function maps an individual input I_i^l to the desired I_i^h , thus cycle-consistent losses are further applied. As illustrated by the green circle in Fig. 1, each real LR image x_i and generators G_{lh}, G_{hl} should satisfy: $I_i^l \rightarrow G_{lh}(I_i^l) \rightarrow G_{hl}(G_{lh}(I_i^l)) \approx I_i^l$. As shown by the blue circle, each real HR image I_j^h and generators G_{lh}, G_{hl} should satisfy: $I_j^h \rightarrow G_{hl}(I_j^h) \rightarrow G_{lh}(G_{hl}(I_j^h)) \approx I_j^h$. The cycle consistent loss is

$$\begin{aligned} \mathcal{L}_{cyc} &= \mathcal{L}_{cyc_lr} + \mathcal{L}_{cyc_hr} \\ &= \mathbb{E}_{I_i^l \sim P(I^l)} \|G_{hl}(G_{lh}(I_i^l)) - I_i^l\|_1 + \mathbb{E}_{I_j^h \sim P(I^h)} \|G_{lh}(G_{hl}(I_j^h)) - I_j^h\|_1. \end{aligned} \quad (5)$$

For the two generators, we minimize the following objective

$$\mathcal{L}_G = \alpha \mathcal{L}_{G_{hl}} + \beta \mathcal{L}_{G_{lh}} + \eta \mathcal{L}_{cyc}, \quad (6)$$

where α, β, η are positive values. To train discriminator D_h and D_l , we minimize

$$\mathcal{L}_D = \mathcal{L}_{D_l} + \mathcal{L}_{D_h}. \quad (7)$$

3 Experiments

We evaluate our framework on two popular EM data sets, FIB-25 [19] and Cremi [11], which can be used as simulated anisotropic images and real anisotropic images, respectively. We employ the Adam optimizer [13] with $\beta_1 = 0.5$, $\beta_2 = 0.999$. The initial learning rate of generators is set to 2×10^{-4} and then decreases by a factor of 0.98 for every epoch. The discriminators are trained with fixed learning rate of 10^{-4} . We implement the proposed framework with PyTorch by using a Titan XP GPU.

Table 1. Quantitative (PSNR/SSIM) comparisons on the axial (xz/yz) slices of FIB-25 dataset. Bold is the best and italic is the second best performance. Note that ‘Cubic’ is the ideal case where the exactly matched degradation is used for supervised training.

Method	Interp	DRCNet				Isonet-2			
		Take	Gau	Ours	Cubic	Take	Gau	Ours	Cubic
xz	25.93	22.97	25.98	<i>26.58</i>	26.85	22.91	25.96	<i>26.56</i>	26.81
	0.652	0.523	0.643	<i>0.678</i>	0.696	0.560	0.648	<i>0.679</i>	0.692
yz	25.93	23.00	25.99	<i>26.57</i>	26.86	22.87	26.01	<i>26.58</i>	26.83
	0.644	0.518	0.635	<i>0.670</i>	0.688	0.551	0.642	<i>0.672</i>	0.685

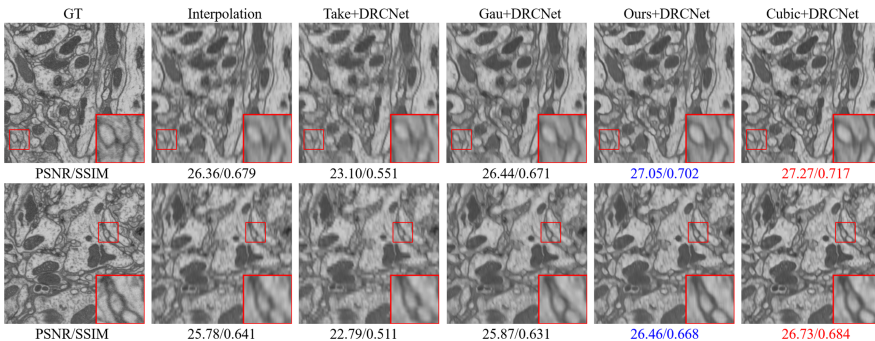


Fig. 2. Visual comparisons on FIB-25 dataset. Best viewed in electronic format.

Evaluation on Simulated Anisotropic Images. To investigate whether the degradation network can learn the correct degradation process, we conduct experiments on simulated anisotropic images. Different from most existing EM data sets, FIB-25 [19] contains isotropic data from the drosophila brain obtained with the FIB-SEM technique. We use a sub-volume ($500 \times 500 \times 500$) from the FIB-25 data set for our experiments. We simulate anisotropic ssTEM images by down-sampling the isotropic images by a factor of 10 along the axial direction using cubic down-sample operation at first, which results in an anisotropic 3D volume with a resolution of $500 \times 500 \times 50$. To verify the effectiveness of our framework, we adopt two reconstruction networks (DRCNet and Isonet-2 [20]) in the experiments. Each reconstruction network is trained in two ways: one is trained in an unsupervised manner using our framework, and the other is trained in a supervised manner using the lateral slices paired with their artificially down-scaled ones. For our unsupervised training, the axial (xz/yz) slices (with a resolution of 500×50) and the lateral (xy) slices (with a resolution of 500×500) of the simulated anisotropic volume are used as training data. For the supervised training, we generate three training data sets to represent different kinds of degradation assumptions. Specifically, the HR ground-truth lateral slices are down-scaled by taking every 10th row, down-scaled using the cubic down-sample operation or firstly blur by a gaussian kernel and then down-scaled

Table 2. Segmentation results on the restored isotropic images. Lower is better.

Method	Interp	DRCNet			
		Take	Gau	Ours	Cubic
VOI	5.88	6.03	5.87	4.98	5.08

Table 3. Quantitative comparisons on stimulated degraded images.

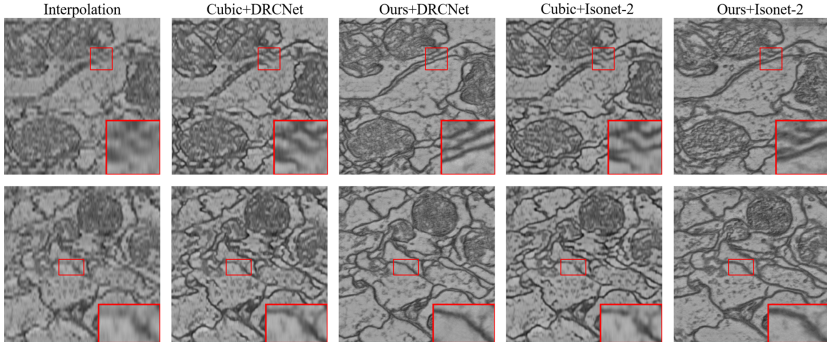
Method	Take	Gau	Ours
PSNR	22.68	29.35	36.55
SSIM	0.716	0.929	0.984

by taking-slice operation. Then, these three kinds of paired HR-LR data are used to train the reconstructed network in a supervised manner. After training, the network models corresponding to different degradation processes can be obtained. At the testing phase, for all methods, *only* the axial (xz/yz) slices of the cubic down-sample simulated anisotropic volume are used as testing images.

Table 1 shows PSNR and SSIM results of the above methods. The words ‘Take’ means training on taking-slices degradation assumption, ‘Gau’ means training on gaussian+taking-slices degradation assumption, ‘Ours’ means training with our framework, and ‘Cubic’ means training on cubic degradation assumption (ideal case). As can been seen, our unsupervised framework achieves comparable results with the ideal supervised method ‘Cubic’. This is because our framework can provide training data, which conforms to the correct degradation process, to the reconstruction network. In contrast, the performance of the networks trained on data with mismatched degradation assumptions, i.e., ‘Take’ and ‘Gau’, are even worse than the direct cubic interpolation. This is caused by the degradation mismatch between training and testing data, which is a common problem in self-supervised learning. As shown in Fig. 2, the results produced by our framework are visually close to ‘Cubic’, which is consistent with quantitative assessments. To prove that our framework can learn the correct degradation process, we further calculate the PSNR/SSIM between the cubic down-sampled LR xz/yz slices and those LR xz/yz images generated by our framework. As shown in Table 3, our framework achieves the highest scores, which indicates that our framework is able to generate more realistic LR images.

To validate the effectiveness of our framework in the subsequent analysis tasks, we further conduct segmentation experiments. We use a state-of-the-art neuron segmentation method [6]. First, we train the segmentation network on the isotropic ground truth, and then use the trained model to evaluate on different restored isotropic volumes. We show the results of variation of information (VOI) in Table 2. Our framework achieves the best performance, which is even better than ‘Cubic’ since the adversarial loss we use could benefit segmentation.

Evaluation on Real Anisotropic Images. To evaluate our framework on real anisotropic images, we conduct experiments on the Cremi [11] dataset, which contains EM data of drosophila brain with anisotropic resolution. We use a volume of $1250 \times 1250 \times 125$ for our experiments, where all the lateral (xy) slices and axial (xz/yz) slices are used as training data. As shown in Fig. 3, even when the real degradation is unknown, using our framework

**Fig. 3.** Visual comparisons on Cremi dataset.**Table 4.** Quantitative (PSNR/SSIM) comparisons on the lateral (xy) slices of Cremi dataset. Bold is the best and italic is the second best performance.

Method	DRCNet	Isonet-1	Isonet-2	VDSR	EDSR	RDN	RCAN	Interp
Cubic	23.00	23.16	22.95	23.02	22.80	22.66	22.69	23.31 0.625
	0.624	0.624	0.626	0.623	0.609	0.608	0.609	
Ours	26.06	24.25	26.04	25.81	26.30	<i>26.53</i>	26.74	0.708 0.715
	0.693	0.650	0.694	0.686	0.697	<i>0.708</i>	0.715	

(Ours+DRCNet, Ours+Isonet-2) can still generate promising results as it learns the real degradation. While directly using cubic interpolation fails to recover HR details. Other two methods, Cubic+DRCNet and Cubic+IsoNet-2, which are trained on the assumption of cubic degradation, introduce unrealistic artifacts. This is because the real degradation is not consistent with the artificial one it assumes. In other words, only the learned reconstruction network with accurate degradation modeling can generalize well to real anisotropic images.

To further validate the effectiveness of our framework, we also conduct experiments on the lateral slices of Cremi dataset. Since it is difficult to acquire large amount of isotropic images paired with its real anisotropic ones, we use our framework to generate anisotropic images from real axial degradation. We first generate LR images by performing the degradation network of ‘Ours+DRCNet’ that previously trained on all the lateral (xy) slices of Cremi dataset. These generated LR images are close to real data. Then, we divide these LR images into a training set and a test set. Finally, we fine-tune our framework with different reconstruction networks on the training set. We select above mentioned DRCNet, Isonet-1 [20], Isonet-2 [20] and other four deep learning-based SR methods: VDSR [12], EDSR [15], RDN [25, 26], RCAN [24]. These SR networks are trained with and without our framework, respectively. We modify the pixel shuffle layer to do up-sample operation in a single direction. As shown in Table 4, due to the

degradation mismatch, using SR networks does not produce satisfactory results. While adopting our framework improves performance, i.e., the values in the second row are significantly higher than those in the first row. This means the users can choose any reconstruction network according to the actual situation.

4 Conclusions

In this paper, we propose an effective framework for isotropic restoration of 3D EM images. We achieve this goal by simultaneously learning the degradation and reconstruction processes in an unsupervised manner. Since our framework requires neither external paired training data nor degradation assumptions, it is easy to implement in most practical applications. In the absence of paired data, our framework still shows encouraging performance. Experiments have demonstrated that even though the reconstruction network is trained with unpaired data in our framework, its reconstruction performance is still close to the performance obtained by training with pre-collected paired data.

Acknowledgment. This work was supported in part by Key Area R&D Program of Guangdong Province with grant No. 2018B030338001, the Fundamental Research Funds for the Central Universities under Grant WK2380000002, and the Natural Science Foundation of China (NSFC) under Grant 61901433.

References

1. Bulat, A., Yang, J., Tzimiropoulos, G.: To learn image super-resolution, use a gan to learn how to do image degradation first. In: Ferrari, V., Hebert, M., Sminchisescu, C., Weiss, Y. (eds.) ECCV 2018. LNCS, vol. 11210, pp. 185–200. Springer, Cham (2018). https://doi.org/10.1007/978-3-030-01231-1_12
2. Chen, C., Xiong, Z., Tian, X., Zha, Z.J., Wu, F.: Camera lens super-resolution. In: Proceedings of the IEEE Conference on Computer Vision and Pattern Recognition, pp. 1652–1660 (2019)
3. Chen, C., Xiong, Z., Tian, X., Zha, Z.J., Wu, F.: Real-world image denoising with deep boosting. *IEEE Trans. Pattern Anal. Mach. Intell.* (2019)
4. Chen, Y., Shi, F., Christodoulou, A.G., Xie, Y., Zhou, Z., Li, D.: Efficient and accurate mri super-resolution using a generative adversarial network and 3d multi-level densely connected network. In: Frangi, A., Schnabel, J., Davatzikos, C., Alberola-López, C., Fichtinger, G. (eds.) MICCAI 2018. LNCS, vol. 11070, pp. 91–99. Springer, Cham (2018). https://doi.org/10.1007/978-3-030-00928-1_11
5. Çiçek, Ö., Abdulkadir, A., Lienkamp, S.S., Brox, T., Ronneberger, O.: 3d u-net: learning dense volumetric segmentation from sparse annotation. In: Ourselin, S., Joskowicz, L., Sabuncu, M., Unal, G., Wells, W. (eds.) MICCAI 2016. LNCS, vol. 9901, pp. 424–432. Springer, Cham (2016)
6. Funke, J., et al.: Large scale image segmentation with structured loss based deep learning for connectome reconstruction. *IEEE Trans. Pattern Anal. Mach. Intell.* **41**(7), 1669–1680 (2018)
7. Goodfellow, I., et al.: Generative adversarial nets. In: Advances in Neural Information Processing Systems, pp. 2672–2680 (2014)

8. Hayworth, K.J., et al.: Ultrastructurally smooth thick partitioning and volume stitching for large-scale connectomics. *Nat. Methods* **12**(4), 319 (2015)
9. He, K., Zhang, X., Ren, S., Sun, J.: Deep residual learning for image recognition. In: IEEE Conference on Computer Vision and Pattern Recognition, pp. 770–778 (2016)
10. Heinrich, L., Bogovic, J.A., Saalfeld, S.: Deep learning for isotropic super-resolution from non-isotropic 3d electron microscopy. In: International Conference on Medical Image Computing and Computer-Assisted Intervention, pp. 135–143 (2017)
11. Funke, J., Saalfeld, S.: D.B.S.T.E.P.: cremi.org/
12. Kim, J., Kwon Lee, J., Mu Lee, K.: Accurate image super-resolution using very deep convolutional networks. In: IEEE Conference on Computer Vision and Pattern Recognition, pp. 1646–1654 (2016)
13. Kingma, D.P., Ba, J.: Adam: a method for stochastic optimization. arXiv preprint [arXiv:1412.6980](https://arxiv.org/abs/1412.6980) (2014)
14. Ledig, C., et al.: Photo-realistic single image super-resolution using a generative adversarial network. In: IEEE Conference on Computer Vision and Pattern Recognition, pp. 4681–4690 (2017)
15. Lim, B., Son, S., Kim, H., Nah, S., Mu Lee, K.: Enhanced deep residual networks for single image super-resolution. In: IEEE Conference on Computer Vision and Pattern Recognition Workshops, pp. 136–144 (2017)
16. Mao, X., Li, Q., Xie, H., Lau, R.Y., Wang, Z., Paul Smolley, S.: Least squares generative adversarial networks. In: IEEE International Conference on Computer Vision, pp. 2794–2802 (2017)
17. Mikula, S.: Progress towards mammalian whole-brain cellular connectomics. *Front. Neuroanat.* **10**, 62 (2016)
18. Ronneberger, O., Fischer, P., Brox, T.: U-net: convolutional networks for biomedical image segmentation. In: Navab, N., Hornegger, J., Wells, W., Frangi, A. (eds.) MICCAI 2015. LNCS, vol. 9351, pp. 234–241. Springer, Cham (2015). https://doi.org/10.1007/978-3-319-24574-4_28
19. Takemura, S., et al.: Synaptic circuits and their variations within different columns in the visual system of drosophila. *Natl. Acad. Sci.* **112**(44), 13711–13716 (2015)
20. Weigert, M., Royer, L., Jug, F., Myers, G.: Isotropic reconstruction of 3d fluorescence microscopy images using convolutional neural networks. In: International Conference on Medical Image Computing and Computer-Assisted Intervention, pp. 126–134 (2017)
21. Weigert, M., et al.: Content-aware image restoration: pushing the limits of fluorescence microscopy. *Nat. Methods* **15**(12), 1090 (2018)
22. Yuan, Y., Liu, S., Zhang, J., Zhang, Y., Dong, C., Lin, L.: Unsupervised image super-resolution using cycle-in-cycle generative adversarial networks. In: IEEE Conference on Computer Vision and Pattern Recognition Workshops, pp. 701–710 (2018)
23. Zhang, K., Zuo, W., Chen, Y., Meng, D., Zhang, L.: Beyond a gaussian denoiser: residual learning of deep cnn for image denoising. *IEEE Trans. Image Process.* **26**(7), 3142–3155 (2017)
24. Zhang, Y., Li, K., Li, K., Wang, L., Zhong, B., Fu, Y.: Image super-resolution using very deep residual channel attention networks. In: Ferrari, V., Hebert, M., Sminchisescu, C., Weiss, Y. (eds.) ECCV 2018. LNCS, vol. 11211, pp. 286–301. Springer, Cham (2018). https://doi.org/10.1007/978-3-030-01234-2_18
25. Zhang, Y., Tian, Y., Kong, Y., Zhong, B., Fu, Y.: Residual dense network for image super-resolution. In: IEEE Conference on Computer Vision and Pattern Recognition, pp. 2472–2481 (2018)

26. Zhang, Y., Tian, Y., Kong, Y., Zhong, B., Fu, Y.: Residual dense network for image restoration. *IEEE Trans. Pattern Anal. Mach. Intell.* (2020)
27. Zhao, C., Carass, A., Dewey, B.E., Prince, J.L.: Self super-resolution for magnetic resonance images using deep networks. In: *IEEE 15th International Symposium on Biomedical Imaging (ISBI 2018)*, pp. 365–368 (2018)
28. Zhao, C., et al.: A deep learning based anti-aliasing self super-resolution algorithm for MRI. In: Frangi, A.F., Schnabel, J.A., Davatzikos, C., Alberola-López, C., Fichtinger, G. (eds.) *MICCAI 2018. LNCS*, vol. 11070, pp. 100–108. Springer, Cham (2018). https://doi.org/10.1007/978-3-030-00928-1_12
29. Zhao, T., Zhang, C., Ren, W., Ren, D., Hu, Q.: Unsupervised degradation learning for single image super-resolution. *arXiv preprint arXiv:1812.04240* (2018)
30. Zhu, J.Y., Park, T., Isola, P., Efros, A.A.: Unpaired image-to-image translation using cycle-consistent adversarial networks. In: *IEEE International Conference on Computer Vision*, pp. 2223–2232 (2017)